

Thermal oxidation of polycrystalline tungsten nanowire

G. F. You and John T. L. Thong^{a)}

Department of Electrical and Computer Engineering, National University of Singapore,
4 Engineering Drive 3, Singapore 117576

(Received 25 February 2010; accepted 20 September 2010; published online 4 November 2010)

The progressive oxidation of polycrystalline tungsten nanowires with diameters in the range of 10–28 nm is studied. The structure and morphology of the tungsten and tungsten oxide nanowires were investigated in detail by transmission electron microscopy. By observing changes in the oxide-shell thickness, a self-limiting oxidation mechanism was found to retard the oxidation rate. Surface reaction and the oxygen diffusion effects were considered in order to understand the influence of stress on the oxidation process. © 2010 American Institute of Physics.
[doi:10.1063/1.3504248]

I. INTRODUCTION

Metal oxide semiconductors stand out as one of the most versatile class of materials, due to their diverse properties and functionality. One-dimensional (1D) nanostructures of such materials continue to gain attention because of their unique electrical, optical, and chemical sensing properties^{1–3} associated with their highly anisotropic geometry and size confinement. They are good candidates for lithium-ion batteries, catalysts, electrochromic devices, and gas sensors.^{4–8} As such, they demonstrate promise for future nanoscale electronic, optoelectronic, and sensing applications.

Among such metal oxides, tungsten oxide 1D nanostructures have been used to construct flat panel displays, optical modulators, gas sensors, humidity/temperature sensors, and so forth.^{9–15} Motivated by potential applications, different techniques for the synthesis of 1D tungsten oxide nanostructure have been developed.^{16–19} One of the simplest and most direct ways to synthesize 1D tungsten oxide nanostructures is through thermal oxidation of tungsten. The oxidation kinetics of the bulk tungsten (W) surface have already been well investigated for over a century.^{20–23} However, limited attention has been paid to the oxidation kinetics of W nanowires although such knowledge is important to achieve precise control of the oxide thickness and microstructure to optimize the performance of tungsten oxide nanowire devices.

We have previously demonstrated the ability to grow single W nanowires through a field-emission induced growth (FEIG) process in the presence of an organometallic precursor.²⁴ Such a nanowire consists of a polycrystalline tungsten core that is covered by a thin carbonaceous coating. Through this technique, a single metallic nanowire could be grown at a predetermined location, which leads to applications such as nanotips for scanning probe microscopy and nanowire interconnects.^{25–27}

In the present work, the oxidation of FEIG tungsten nanowires by direct annealing in an oxygen environment is investigated. The mechanism of oxidation and investigations into the morphology of the tungsten oxide nanowire will be

discussed. The objective of the current work is to provide an understanding of how oxidation kinetics is modified in a 1D nanowire geometry.

II. EXPERIMENT

Tungsten nanowires were first grown on a micromachined silicon nitride membrane die that fits into a standard 3 mm transmission electron microscope (TEM) grid holder. These dies contain bond pads at the periphery and gold-on-titanium electrodes that lead into the vicinity of the suspended 50 nm thick nitride membrane (Fig. 1). The gold electrodes serve a dual purpose. For the FEIG process, one grounded electrode (cathode) is needed from which the nanowire grows. The growth details of the tungsten nanowire can be found in previous work.^{28,29} On the other hand, in directing the nanowire to grow over the other electrodes, two-point or four-point electrical measurements can subsequently be made on the bridging nanowire. Later, a focused ion beam was used to etch several hollow slots (of approximately 5 μm width) in the membrane, between the elec-

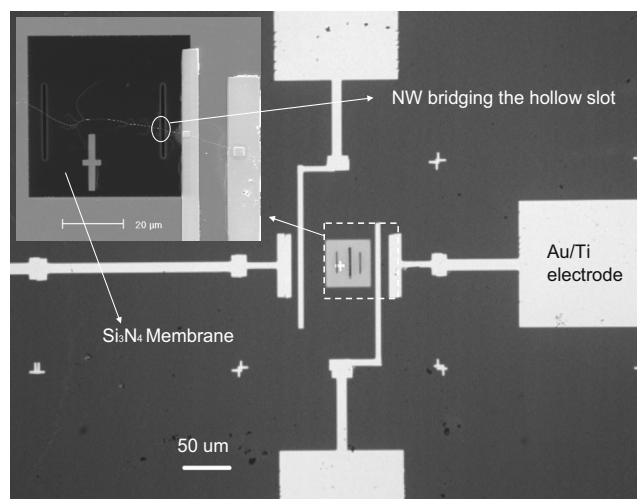


FIG. 1. Micrograph of prepared TEM sample coated with electrode patterns. Inset SEM image shows nanowire grown on top of the Si_3N_4 membrane.

^{a)}Electronic mail: elett1@nus.edu.sg.

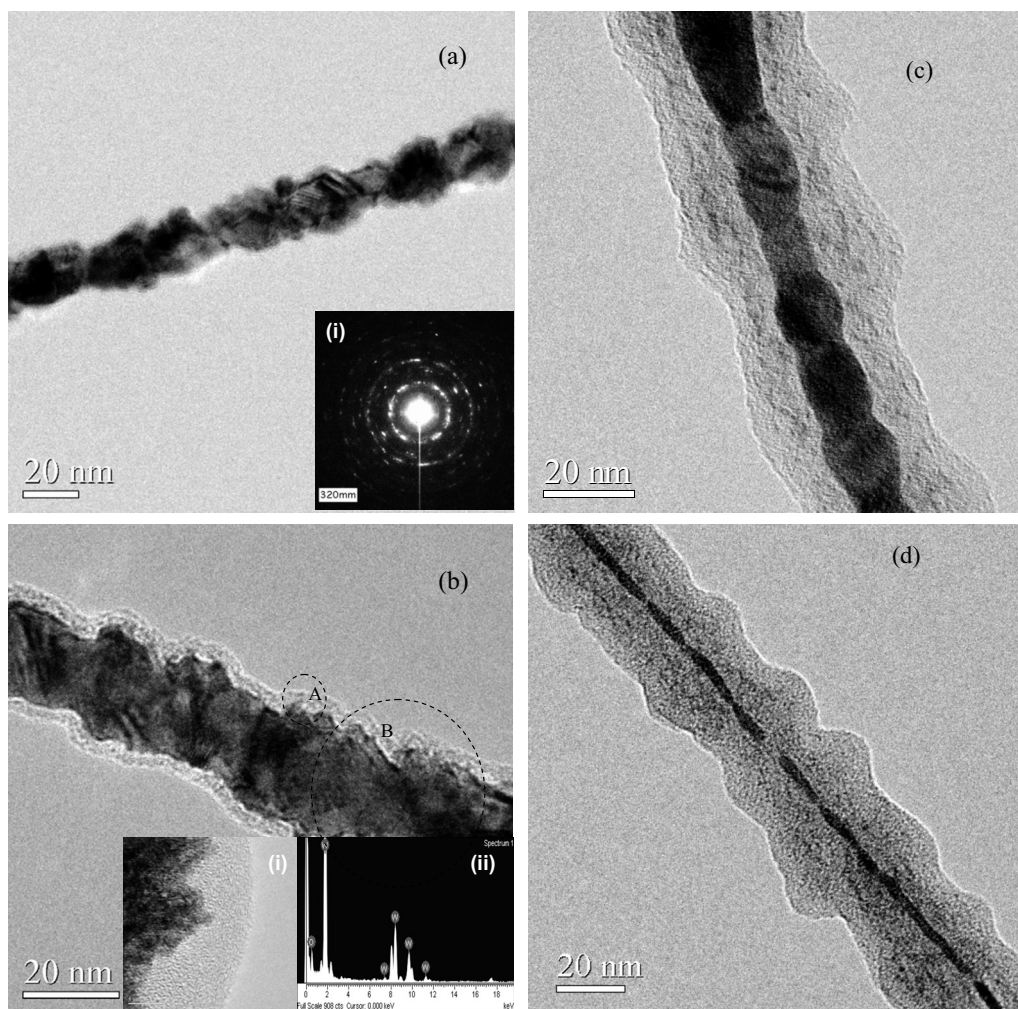


FIG. 2. (a) TEM image of W nanowire with an average diameter of 25 nm, inset (i) shows the selective diffraction pattern. (b) Nanowire oxidized for 1 h, inset (i) shows HRTEM image for area A and inset (ii) is the EDX spectrum for area B. (c) and (d) are TEM images of nanowire after oxidation for 4 and 12 h.

trodes which lie outside the membrane. These slots allow unobscured imaging of the straddling nanowires by the TEM electron beam.

The polycrystalline tungsten nanowire grown on the electrodes was then placed on a button heater in a vacuum chamber with a base pressure of 10^{-6} mbar for thermal oxidation. The temperature was measured using a miniature (200 μm) Type-K thermocouple in direct contact with the surface of the silicon nitride membrane die. To ensure accurate temperature measurement of the specimen, good thermal contact between the die surface and thermocouple was achieved through the use of silver paint at the point of contact. Oxidation was carried out at temperatures ranging from 400 to 500 $^{\circ}\text{C}$ by admitting oxygen at 10^{-2} mbar.

III. RESULT AND DISCUSSION

A. Changes in morphology during oxidation

Five tungsten nanowires with diameters ranging from 10 to 28 nm were individually grown on different silicon nitride membrane TEM dies. Prior to oxidation, each tungsten nanowire was first imaged by high-resolution TEM (HRTEM, Philips CM300) to determine the core diameter. Due to the

rough surface of the nanowire, the uniformity of diameter along the wire length is poor. For example, Fig. 2(a) shows a TEM image of a typical tungsten nanowire before oxidation. The diameter of an individual nanowire can range from 22 to 30 nm. Therefore a mean value was obtained by taking ten random readings along the nanowire. The mean diameter is about 25 nm with a standard deviation of 3.2 nm. In our previous studies, it was found that the tungsten nanowire is a polycrystalline aggregate with highly crystalline grains along the nanowire. Inset image (i) is an indexed selected area diffraction pattern.

After oxidation for a period of time, the nanowire specimen was taken out for TEM characterization. Figure 2(b) shows the oxidized nanowire after oxidation for 1 h. Strong diffraction and mass-contrast is observed in the bright-field image, which shows the existence of two phases of different weight and degree of crystallinity in the specimen. It is suggested that the denser phase is tungsten which constitutes the cylindrical core, while the less dense phase is tungsten oxide that encapsulates the core. This can be confirmed by the HRTEM phase-contrast image [inset image (i)], which corresponds to the interface area A between the core and overcoat shell. In image (i), the detected lattice spacing of the

core is about 0.225 nm, which corresponds to the tungsten {110} planes. The overcoat shell layer appears to be amorphous. In order to determine its chemical nature, energy-dispersive x-ray (EDX) spectroscopy for selected area B was carried out. The result [inset image (ii)] reveals that the region comprises mainly oxygen and tungsten. From the EDX spectrum, the atomic weight ratio of the detected tungsten to oxygen (W:O) is about 95:5. Compared to the EDX spectrum of the nanowire before oxidation in which the peak of oxygen signal could not be identified, the additional oxygen content in the oxidized nanowire is believed to come from reacted tungsten oxide in the overcoat shell region.

To monitor the progress of oxidation, the diameters of the tungsten core and thickness of oxide shell were measured after various cumulative oxidation times. Figure 2(c) is a TEM image of nanowire after 4 h of oxidation, clearly showing that with the increase in oxidation time, the average diameter of the tungsten core has reduced to ~ 14 nm while the oxide layer thickness has expanded to ~ 15 nm. Finally after 12 h of oxidation, the tungsten core has reduced to ~ 4 nm in diameter while the oxide thickness is ~ 23 nm [Fig. 2(d)].

It is observed, first, that the oxide layer becomes increasingly nonuniform with oxidation time, which could have arisen from differences in oxidation rates for different tungsten crystallographic orientations along the polycrystalline nanowire,³⁰ and exacerbated by the volume expansion of the oxide. In addition, oxidation preferentially occurs at the boundaries and defects,³¹ which could give rise to nonconformal oxidation along the nanowire.

On the other hand, the tungsten core became increasingly uniform in diameter, and appears smooth after 12 h of oxidation. This phenomenon can be attributed to the effect of compressive stress in the oxide. In general, compressive stress arises in a growing oxide when its molar volume exceeds that of the material being oxidized.³² In the case of tungsten oxide, the volume of a WO_3 molecule is 32.37 \AA^3 , which is larger than the volume of a tungsten atom of 9.53 \AA^3 . Thus a large increase in molar volume accompanies the conversion of W to WO_3 or even a suboxide. During oxidation of the tungsten, the oxygen diffuses through the previously-formed oxide layer and reacts with the tungsten atoms at the tungsten/oxide interface. The newly-formed oxide has to push out the previously-formed oxide to accommodate the volume expansion. This results in compressive stress accumulating at the tungsten oxide interface, which may limit the oxygen-tungsten reaction rate and/or the diffusion rate of oxidants to the interface.^{33,34} As a consequence, the rate of reduction in the core diameter becomes progressively smaller and finally the core approaches an asymptotically uniform diameter as shown in Fig. 2(d). This retarded oxidation phenomenon is termed as self-limiting (or “stress-limited”) oxidation which has been widely studied in Si nanowires.^{35–37} It has also been observed in the oxidation of metal nanowires of tin³¹ and bismuth,³⁸ as well as in nanodot structures.^{39,40} However, to the best of our knowledge, the self-limiting oxidation of tungsten nanowire has not been observed nor studied previously.

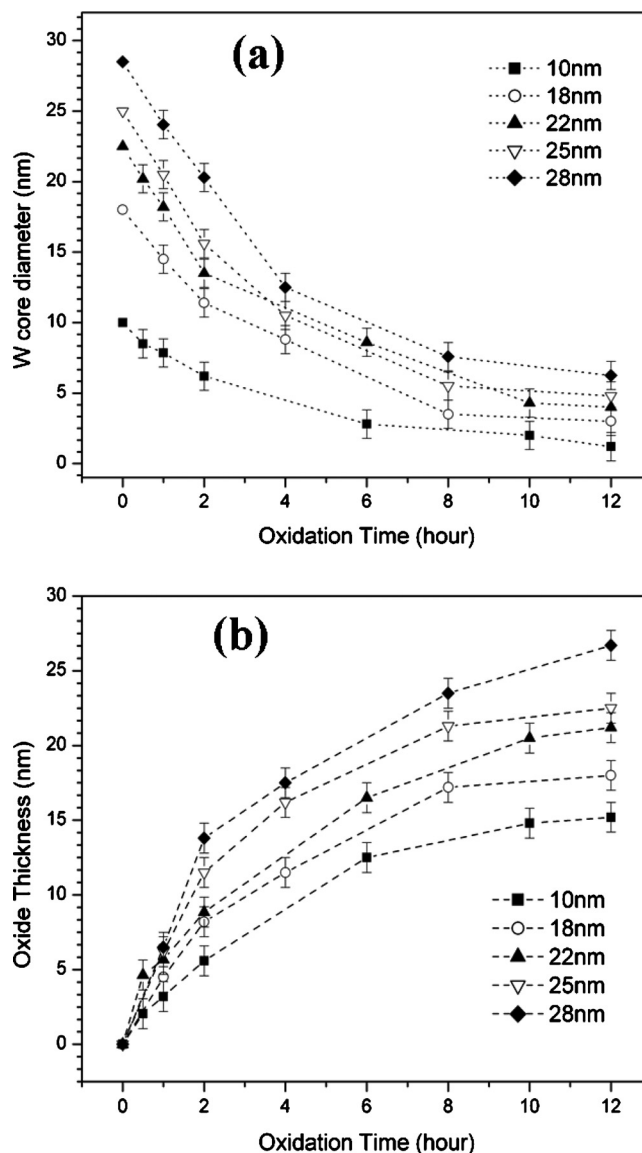


FIG. 3. (a) Tungsten core diameter and (b) tungsten oxide shell thickness as a function of oxidation time for different nanowires.

The remaining diameter of the tungsten core and thickness of oxide shell as a function of oxidation time for different nanowires are plotted as shown in Figs. 3(a) and 3(b), respectively. For oxidation beyond ~ 6 h, the oxide growth rate and the shrinkage rate of the core progressively diminishes with time. After oxidation for about 12 h, both thickness of oxide shell and diameter of tungsten core appear to approach asymptotic values, as would be expected if the oxidation in tungsten nanowire is self-limited by oxidation-induced stress.

B. Self-limiting oxidation

At the outset, we need to determine whether the self-limiting oxidation is kinetically limited or thermodynamically limited. Assuming self-limiting oxidation will reach a constrained equilibrium state, although a residual tungsten core cannot be the lowest energy state since the oxidation reaction is highly exothermic, a deep metastable state of constrained equilibrium may, in principle, occur if a large energy

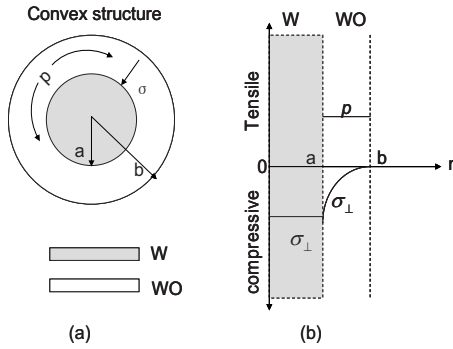


FIG. 4. Stress components in a convex tungsten oxide nanowire structure during oxidation.

barrier exists in the pathway to equilibrium. To assess the likelihood of this metastable state, the incremental energy cost arising from stress built up in the oxide and the formation energy of WO_3 from W is compared. A simple elastic model yields an upper bound for the strain energy per unit column length, $\pi Y \delta^2 / 2(1-\nu)$, where Y and ν are the Young's modulus and the Poisson's ratio of the oxide, respectively, and δ is the radial expansion at the W/WO_3 interface due to the additional oxide growth. From this estimation, taking Y as about ~ 300 GPa (Refs. 41 and 42) and ν as 0.2 from bulk oxide values,⁴³ the upper bound of energy cost per oxide molecule grown for a tungsten core diameter of 2 nm and 5 nm is estimated to be in the order 0.4 eV and 0.1 eV, respectively, which is much smaller than the 9 eV energy gained for each oxide molecule created due to the chemical reaction. Therefore a constrained equilibrium state should be ruled out. It can be concluded that oxidation of W wire is kinetically limited and the asymptotic behavior arises from accumulated interfacial stress.

To explain the oxidation process in a cylindrical Si structure under interfacial stress, Kao *et al.*^{44,45} proposed a model where the effects of mechanical stress on the reduction in oxidation rate at the Si/SiO_2 interface are taken into account. In this work, Kao's model⁴⁵ is applied to explain the self-limiting oxidation mechanism in tungsten nanowires which can be described as follows.

While extending the Deal–Grove⁴⁶ approach with appropriate boundary conditions in cylindrical coordinates, the oxidation rate (dx_0/dt) can be expressed as:

$$N \frac{dx_0}{dt} = \frac{C^*}{\frac{1}{K_s} + \frac{1}{h} \frac{a}{b} + \frac{1}{D} a \log \frac{b}{a}}, \quad (1)$$

where K_s is the surface reaction coefficient, D is the oxidant diffusivity in oxide, C^* is the oxidant solubility in the oxide, N is the number of oxidants required to form one unit volume of oxide, h is the surface mass transfer constant of the oxidant ($1/h \ll 1/K_s$, and can be neglected), and a and b are the radius of curvature of the tungsten core surface and the radius of oxide shell surface, respectively [Fig. 4(a)]. Both a and b change with oxidation time.

The formation of new oxide at the tungsten surface involves a volume expansion. The newly-formed oxide expands and pushes out the old oxide, which rearranges itself

through viscous flow. Because of the high viscosity (η) of the oxide, the viscous oxide deformation involves large stresses,⁴⁷ which can be resolved into σ_\perp , the stress normal to the W/WO interface, and p , the hydrostatic pressure throughout the bulk of oxide [as shown in Fig. 4(a)]. The stress components in a convex cylindrical structure are shown schematically in Fig. 4(b).⁴⁵ σ_\perp is compressive and can be expressed as:

$$\sigma_\perp = 2\eta\xi \left(\frac{1}{a^2} - \frac{1}{b^2} \right), \quad (2)$$

while p is tensile and can be expressed as:

$$p = -2\eta\xi \frac{1}{b^2}, \quad (3)$$

where ξ is a velocity constant determined from the oxide growth rate at the interface.

According to Kao's model,⁴⁵ the stress-dependent parameters in Eq. (1) are reaction rate at the interface K_s , oxidant diffusivity D , and oxidant solubility C^* . As suggested by Sutardja and Oldham,⁴⁸ C^* in silicon oxidation is almost independent of stress if the oxidation temperature is low (< 800 °C). In the present study, since both oxidant concentration and oxidizing temperature are low, we can assume the oxygen solubility C^* in amorphous tungsten oxide to be a stress-independent constant parameter. It was suggested by Kao⁴⁵ and Umimoto⁴⁹ that the viscosity of oxide is a function of the temperature T and hydrostatic pressure p . Sutardja and Oldham⁴⁸ modified it by considering the viscosity as a shear stress dependent parameter.

Sutardja's model predicted that the viscosity is almost constant over a large range of shear stress and falls beyond a certain critical high value of shear stress. Since the shear stress decreases with an increase in oxide thickness, in the present experiment, the viscosity η is assumed to remain constant at 400 °C.

Therefore, only K_s and D are considered as stress-dependent parameters during tungsten oxidation in our experiments. Again, as proposed by Kao *et al.*⁴⁵ and Sutardja and Oldham,⁴⁸ both parameters have an Arrhenius relationship with stress barriers as follows:

$$K_s = K_0 \exp\left(-\frac{\sigma_\perp V_k}{k_B T}\right), \quad (4)$$

and

$$D = D_0 \exp\left(-\frac{pV_d}{k_B T}\right), \quad (5)$$

where K_0 is the stress-free reaction rate constant, D_0 is the oxidant diffusivity, k_B is Boltzmann's constant. V_k is the volume change corresponding to a unit chemical oxidation reaction. V_d is the activation volume of diffusivity.

To understand the stress contribution to the retardation of the oxidation rate, two kinds of the self-limiting oxidation are studied, namely, (1) reaction-limited oxidation where oxidation is retarded only by the effect of stress on the interface reaction, ($p=0$) and (2) diffusion-limited oxidation where oxidation is influenced only by the hydrostatic pres-

TABLE I. Reference values used in simulation.

C^*	N	η	D_0	K_0
7.5×10^{-5} (molecules/nm ³)	16.5 (molecules/nm ³)	2.5 (centistokes)	1.3 (cm ² /s)	0.5 (Å/s)
50	51	52	53	54

sure in oxide ($\sigma_{\perp}=0$). To simulate the self-limiting oxidation of the tungsten nanowire structure at 400 °C, the initial conditions are established as follows:

- (i) The initial value of geometric parameters a , b , and ξ are determined from TEM measurements.
- (ii) For reaction-limited oxidation, it is assumed that $p=0$ and $D=D_0$ while for diffusion-limited oxidation, the normal stress σ_{\perp} is ignored ($\sigma_{\perp}=0$) and $K=K_0$. D_0 and K_0 are stress-free constants (see Table I).
- (iii) In silicon oxidation,⁴⁸ V_k and V_d are considered as constant parameters during oxidation. In this work, V_k and V_d are determined by curve fitting to the first experimental data point of each nanowire under reaction-limited and diffusion-limited oxidation conditions, respectively (Fig. 3). The values obtained for V_k and V_d are then used to calculate K_s and D , respectively, for this nanowire at other times according to Eqs. (4) and (5). σ_{\perp} and p are calculated through Eqs. (2) and (3).
- (iv) The oxide thickness under reaction-limited and diffusion-limited oxidation conditions are calculated using Eq. (1), with the reference values for tungsten oxide, C^* , N , and η as listed in Table I. Finally the calculation results are shown in Figs. 5(a) and 5(b).

For reaction-limited oxidation [Fig. 5(a)], the simulated oxide thicknesses are lower than the experimental values. This means that in the absence of any influence from hydrostatic pressure in the oxide, the oxidation process would be more retarded due to the accumulating normal stress, σ_{\perp} , at the tungsten/oxide interface, which reduces the reaction rate, K_s , by making the oxidation reaction less energetically favorable. The difference in oxide thickness between simulation and experiment is greater for a thicker nanowire, which could be attributed to the higher normal stress accumulated in the thicker nanowire. Figure 5(a) indicates a trend where the normal compressive stress at the tungsten/oxide interface retards tungsten oxidation.

On the other hand, a comparison of the simulation results under diffusion-limited conditions with the experimental values shows that the oxidation process is faster in the absence of any influence from normal compressive stress at the tungsten/oxide interface [Fig. 5(b)]. This is because in a convex nanowire structure, the hydrostatic pressure p is tensile throughout the oxide [Fig. 4(b)]. As tensile pressure would enhance the volume of the voids in the oxide network that are occupied by the diffusing oxidant species,³⁴ the oxidation rate increases.

Combining the results of Figs. 5(a) and 5(b), it can be added that the oxidation is neither fully reaction rate lim-

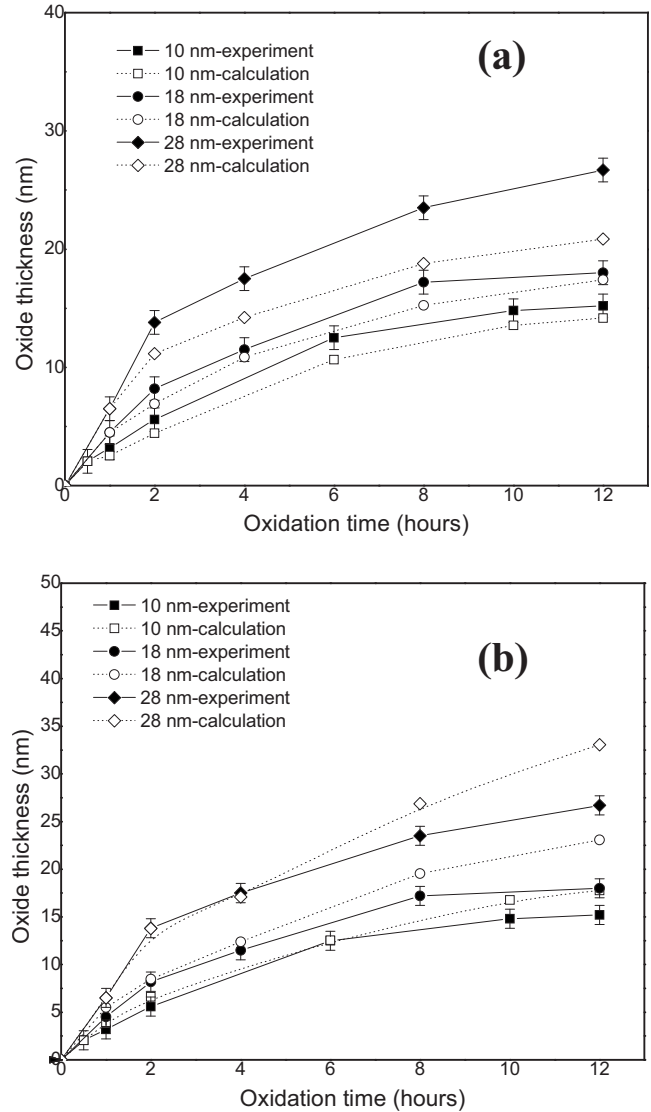


FIG. 5. Simulated oxide thickness assuming (a) reaction-limited oxidation, and (b) diffusion-limited oxidation compared with experimental data.

ited, nor fully diffusion-rate limited. Both the normal compressive stress σ_{\perp} at the tungsten/oxide interface and tensile hydrostatic pressure p in the oxide play a role in the oxidation, in which the former retards the oxidation reaction rate while the latter enhances oxidant diffusion in the oxide. These two opposing stress influences give rise to the oxidation trend observed (Fig. 3).

IV. CONCLUSION

In summary, amorphous tungsten oxide nanowires were obtained through thermal oxidation of the tungsten nanowire at a temperature of about 400 °C in a low pressure oxygen environment. It was found that oxidation is self-limited by accumulated stress in the oxide, which results in an amorphous tungsten/tungsten oxide core-shell structure. Nonuniformity of the oxide shell may be due to anisotropy in the oxidation rate of different crystal planes. The uniformity of the tungsten core after a period of oxidation may be attributed to the retardation of the oxidation rate. The simulations based on Kao's model show that self-limiting oxidation is

mainly due to a combined effect from normal compressive stress at the tungsten/oxide interface and tensile hydrostatic pressure in the oxide where the oxidation reaction rate is retarded by compressive normal stress and oxidant diffusion is enhanced by tensile hydrostatic pressure.

- ¹P. Poizot, S. Laruelle, S. Grugeon, L. Dupont, and J.-M. Tarascon, *Nature (London)* **407**, 496 (2000).
- ²J. G. Lu, P. Chang, and Z. Y. Fan, *Mater. Sci. Eng. R.* **52**, 49 (2006).
- ³G. Z. Shen, P. C. Chen, K. Ryu, and C. W. Zhou, *J. Mater. Chem.* **19**, 828 (2009).
- ⁴M. Ponzzi, C. Duschatzky, A. Carrascull, and E. Ponzzi, *Appl. Catal., A* **169**, 373 (1998).
- ⁵A. Talledo and C. G. Granqvist, *J. Appl. Phys.* **77**, 4655 (1995).
- ⁶C. Li, D. Zhang, S. Han, X. Liu, T. Tang, and C. Zhou, *Adv. Mater.* **15**, 143 (2003).
- ⁷Y. L. Wang, X. C. Jiang, and Y. Xia, *J. Am. Chem. Soc.* **125**, 16176 (2003).
- ⁸Y. Kobayashi, H. Hata, M. Salama, and T. E. Mallouk, *Nano Lett.* **7**, 2142 (2007).
- ⁹C. Santato, M. Odziemkowski, M. Ulmann, and J. Augustynski, *J. Am. Chem. Soc.* **123**, 10639 (2001).
- ¹⁰Y. Kolytynin, S. I. Nikitenko, and A. J. Gedanken, *J. Mater. Chem.* **12**, 1107 (2002).
- ¹¹S. H. Wang, T. C. Chou, and C. C. Liu, *Sens. Actuators B* **94**, 343 (2003).
- ¹²Y. S. Kim, S. C. Ha, K. Kim, H. Yang, S.-Y. Choi, Y. T. Kim, J. T. Park, C. H. Lee, J. Choi, J. Paek, and K. Lee, *Appl. Phys. Lett.* **86**, 213105 (2005).
- ¹³A. Ponzoni, E. Comini, G. Sbergeglieli, J. Zhou, S. Z. Deng, N. S. Xu, Y. Ding, and Z. L. Wang, *Appl. Phys. Lett.* **88**, 203101 (2006).
- ¹⁴B. Deb, S. Desai, G. U. Sumanasekera, and M. K. Sunkara, *Nanotechnology* **18**, 285501 (2007).
- ¹⁵S. Gubbala, J. Thangala, and M. K. Sunkara, *Sol. Energy Mater. Sol. Cells* **91**, 813 (2007).
- ¹⁶K. Zhu, H. He, S. Xie, X. Zhang, W. Zhou, S. Jin, and B. Yue, *Chem. Phys. Lett.* **377**, 317 (2003).
- ¹⁷J. Zhou, Y. Ding, S. Z. Deng, L. Gong, N. S. Xu, and Z. L. Wang, *Adv. Mater.* **17**, 2107 (2005).
- ¹⁸Y. Baek and K. Yong, *J. Phys. Chem. C* **111**, 1213 (2007).
- ¹⁹X. Song, Y. Zheng, E. Yang, and Y. Wang, *Mater. Lett.* **61**, 3904 (2007).
- ²⁰E. A. Gulbransen and K. F. Andrew, *J. Electrochem. Soc.* **107**, 619 (1960).
- ²¹W. W. Webb, J. T. Norton, and C. Wagner, *J. Electrochem. Soc.* **103**, 107 (1956).
- ²²Y. G. Ptushinskii and B. A. Chuikov, *Surf. Sci.* **6**, 42 (1967).
- ²³D. A. King, T. E. Madey, and J. T. Yates, *J. Chem. Phys.* **55**, 3236 (1971).
- ²⁴J. T. L. Thong, M. Yeadon, C. H. Oon, and W. D. Zhang, *Appl. Phys. Lett.* **81**, 4823 (2002).
- ²⁵A. B. H. Tay and J. T. L. Thong, *Appl. Phys. Lett.* **84**, 5207 (2004).
- ²⁶A. B. H. Tay and J. T. L. Thong, *Rev. Sci. Instrum.* **75**, 3248 (2004).
- ²⁷C. H. Oon and J. T. L. Thong, *Nanotechnology* **15**, 687 (2004).
- ²⁸C. H. Oon, J. T. L. Thong, Y. Lei, and W. K. Chim, *Appl. Phys. Lett.* **81**, 3037 (2002).
- ²⁹C. H. Oon, S. H. Khong, C. B. Boothroyd, and J. T. L. Thong, *J. Appl. Phys.* **99**, 064309 (2006).
- ³⁰O. V. Mitrofanov, *Z. Kristallogr.* **8**, 229 (1963).
- ³¹A. Kolmakov, Y. Zhang, and M. Moskovits, *Nano Lett.* **3**, 1125 (2003).
- ³²J. Stringer, *Corros. Sci.* **10**, 513 (1970).
- ³³C. H. Hsueh and A. G. Evans, *J. Appl. Phys.* **54**, 6672 (1983).
- ³⁴D. B. Kao, J. P. McVittie, W. D. Nix, and K. C. Saraswat, *Tech. Dig. - Int. Electron Devices Meet.* **1985**, 388.
- ³⁵H. I. Liu, D. K. Biegelsen, N. M. Johnson, F. A. Ponce, and R. F. W. Pease, *J. Vac. Sci. Technol. B* **11**, 2532 (1993).
- ³⁶H. I. Liu, D. K. Biegelsen, F. A. Ponce, N. M. Johnson, and R. F. W. Pease, *Appl. Phys. Lett.* **64**, 1383 (1994).
- ³⁷H. Heidemeyer, C. Single, F. Zhou, F. E. Prins, D. P. Kern, and E. Plies, *J. Appl. Phys.* **87**, 4580 (2000).
- ³⁸L. Li, Y. W. Yang, G. H. Li, and L. D. Zhang, *Small* **2**, 548 (2006).
- ³⁹K. C. Scheer, R. A. Rao, R. Muralidhar, S. Bagchi, J. Conner, L. Lozano, C. Perez, M. Sadd, and B. E. White, *J. Appl. Phys.* **93**, 5637 (2003).
- ⁴⁰C. H. Chen, T. Yamaguchi, K. I. Sugawara, and K. Koga, *J. Phys. Chem. B* **109**, 20669 (2005).
- ⁴¹N. M. G. Parreira, N. J. M. Carvalho, and A. Cavaleiro, *Thin Solid Films* **510**, 191 (2006).
- ⁴²T. Polcar, N. M. G. Parreira, and A. Cavaleiro, *Vacuum* **81**, 1426 (2007).
- ⁴³M. L. Dunn and H. Ledbetter, *J. Mater. Res.* **10**, 2715 (1995).
- ⁴⁴D.-B. Kao, J. P. McVittie, W. D. Nix, and K. C. Saraswat, *IEEE Trans. Electron Devices* **34**, 1008 (1987).
- ⁴⁵D. B. Kao, J. P. McVittie, and W. M. Nix, *IEEE Trans. Electron Devices* **35**, 25 (1988).
- ⁴⁶B. E. Deal and A. S. Grove, *J. Appl. Phys.* **36**, 3770 (1965).
- ⁴⁷E. P. EerNisse, *Appl. Phys. Lett.* **35**, 8 (1979).
- ⁴⁸P. Sutardja and W. G. Oldham, *IEEE Trans. Electron Devices* **36**, 2415 (1989).
- ⁴⁹H. Umimoto, S. Odanak, I. Nakao, and H. Esaki, *IEEE Trans. Comput.-Aided Des.* **8**, 599 (1989).
- ⁵⁰J. B. Batty and R. E. Stickney, *J. Chem. Phys.* **51**, 4475 (1969).
- ⁵¹B. Gerand, G. Nowogrocki, and M. Figlarz, *J. Solid State Chem.* **38**, 312 (1981).
- ⁵²J. A. Bailey, K. D. Budd, and T. T. Tran, U.S. Patent No. 5772978 (30 June 1998).
- ⁵³J. Stringer and A. R. Rosenfield, *Nature (London)* **199**, 337 (1963).
- ⁵⁴E. A. Gulbransen, *Ind. Eng. Chem.* **41**, 1385 (1949).